Article

Mesoporous Polyhedral Cages and Shells Formed by Textured Self-Assembly of ZnO Nanocrystals

Pu Xian Gao, and Zhong Lin Wang

J. Am. Chem. Soc., **2003**, 125 (37), 11299-11305• DOI: 10.1021/ja035569p • Publication Date (Web): 23 August 2003

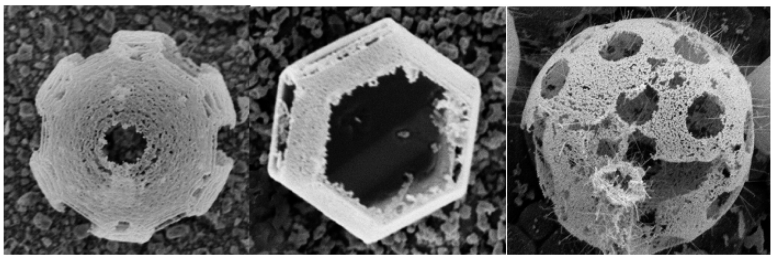

J|A|C|S
ARTICLES
Published on Web 08/23/2003

Mesoporous Polyhedral Cages and Shells Formed by Textured Self-Assembly of ZnO Nanocrystals

Pu Xian Gao and Zhong Lin Wang*

Contribution from the School of Materials Science and Engineering, Georgia Institute of Technology, Atlanta, Georgia 30332-0245

Received April 10, 2003; E-mail: zhong.wang@mse.gatech.edu

Abstract: We report a new structure, mesoporous structured polyhedral drum and spherical cages and shells formed by textured self-assembly of ZnO nanocrystals, which are made by a novel self-assembly process during epitaxial surface oxidation. The cages/shells exhibit unique geometrical shapes, and their walls are composed of mesoporous and textured ZnO nanocrystals. The structures of the cages and shells are studied, and a growth mechanism is proposed to be a process following solidification of the Zn liquid droplets, surface oxidation, and sublimation.

1. Introduction

Conjunction and integration of the self-assembled process and structures with lithography-based nanofabrication techniques are the key to bridging the "bottom-up" with the "top-down" approach in future nanotechnology. As the first step toward this goal, exploration of techniques for building self-assembled nanostructures at all length scales and understanding the growth mechanisms are essential for achieving superior functionality. Biomaterial-like morphologies have been synthesized via self-assembled mesophase materials using the solution-based chemical approach,[1,2] forming a group of structures such as ropes, helixes, spirals, gyroids, doughnuts, and discoids, and even hierarchically ordered mesophase crystals.[3−5] Structures formed by self-assembly of size- and shape-controlled nanocrystals, passivated with surfactant and suspended in solution, have been demonstrated for a wide range of metallic,[6−11] semiconductor,[12−14] and oxide nanocrystals.[15,16]

We report here a new self-assembled nanostructure, mesoporous structured polyhedral cages and shells formed by self-assembly of ZnO, which are made by a novel self-assembly process during physical deposition. The cages/shells exhibit unique geometrical shapes, and their walls are composed of mesoporous and textured ZnO nanocrystals. The structures of the cages and shells are studied, and a growth mechanism is proposed.

2. Materials Synthesis

Zinc oxide is a versatile smart material that has unique applications in catalysts, sensors, piezoelectric transducers and actuators,[17] photovoltaic,[18] and surface acoustic wave devices.[19] Growth of high-quality (0001) textured ZnO thin films has received enormous attention due to its maximized piezoelectric performance.[20] Thin films composed of nanocrystalline ZnO are usually grown by chemical vapor deposition and e-beam sputtering. The structures reported here were synthesized by a solid−vapor deposition process, analogous to the process used for the synthesis of oxide nanobelts.[21] The experimental apparatus includes a horizontal tube furnace, a rotary pump system, and a gas supply system. A mixture of commercial ZnO, SnO_2, and graphite powders in an atomic ratio of 2:1:1 was grounded and then used as the source material, which is located in an alumina boat and positioned at the center of the alumina tube. After the tube was evacuated to 2×10^{-3} Torr, thermal evaporation was conducted at 1150 °C for 15 min under a pressure of 200−300 Torr and an Ar flow rate 25 sccm (standard

(1) Yang, H.; Coombs, N.; Ozin, G. A. *Nature* **1997**, *386*, 692−695.
(2) Zhao, D.; Sun, J.; Li, Q.; Stucky, G. D. *Chem. Mater.* **2000**, *12*, 275−279.
(3) Tian, Z. R. R.; Liu, J.; Voigt, J. A.; McKenzie, B.; Xu, H. F *Angew. Chem., Int. Ed.* **2003**, *42*, 413−417.
(4) Tian, Z. R. R.; Liu, J.; Xu, H. F.; Voigt, J. A.; McKenzie, B.; Matzke, C. M. *Nano Lett.* **2003**, *3*, 179−182.
(5) Fan, H. Y.; Reed, S.; Baer, T.; Schunk, R.; Lopez, G. P.; Brinker, C. J. *Micorporous Mesoporous Mater.* **2001**, *44*, 625−637.
(6) Whetten, R. L.; Khoury, J. T.; Alvarez, M. M.; Murthy, S.; Vezmar, I.; Wang, Z. L.; Stephens, P. W.; Cleveland, C. L.; Luedtke, W. D.; Landman, U. *Adv. Mater.* **1996**, *8*, 428−433.
(7) Collier, C. P.; Saykally, R. J.; Shiang, J. J.; Henrichs, S. E.; Heath, J. R. *Science* **1997**, *277*, 1978−1981.
(8) Pileni, M. P. *Appl. Surf. Sci.* **2001**, *171*, 1−14.
(9) Pileni, M. P. *J. Phys. Chem. B* **2001**, *105*, 3358−3371.
(10) Sun, S. H.; Murray, C. B.; Weller, D.; Folks, L.; Moser, A. *Science* **2000**, *287*, 1989−1992.
(11) Kiely, C. J.; Fink, J.; Brust, M.; Bethell, D.; Schiffrin, D. J. *Nature* **1998**, *396*, 444−446.
(12) Murray, C. B.; Kagan, C. R.; Bawendi, M. G. *Science* **1995**, *270*, 1335−1338.
(13) Peng, X. G.; Manna, L.; Yang, W. D.; Wickham, J.; Scher, E.; Kadavanich, A.; Alivisatos, A. P. *Nature* **2000**, *404*, 59−61.
(14) Braun, P. V.; Osenar, P.; Stupp, S. I. *Nature* **1996**, *380*, 325−328.
(15) Bentzon, M. D.; Wonterghem, J. V.; Mrup, S.; Thölen, A.; Koch, C. J. W. *Philos. Mag. B* **1989**, *60*, 169−178.
(16) Yin, J. S.; Wang, Z. L. *Phys. Rev. Lett.* **1997**, *79*, 2570−2573.
(17) Minne, S. C.; Manalis, S. R.; Quate, C. F. *Appl. Phys. Lett.* **1995**, *67*, 3918−3920.
(18) Keis, K.; Vayssieres, L.; Lindquist, S.; Hagfeldt, A. *Nanostruct. Mater.* **1999**, *12*, 487−490.
(19) Gorla, C. R.; Emanetoglu, N. W.; Liang, S.; Mayo, W. E.; Lu, Y.; Wraback, M.; Shen, H. *J. Appl. Phys.* **1999**, *85*, 2595−2602.
(20) Bernardini, F.; Fiorentini, V.; Vanderbilt, D. *Phys. Rev. B* **1997**, *56*, 10024−10027. The theoretically calculated piezoelectric coefficients for ZnO are $e_{33} = 0.89$, $e_{31} = -0.51$ C/m^2. The experimentally measured coefficient is $e_{33} = 1.0-1.2$ C/m^2.
(21) Pan, Z. W.; Dai, Z. R.; Wang, Z. L. *Science* **2001**, *291*, 1947−1949.

10.1021/ja035569p CCC: $25.00

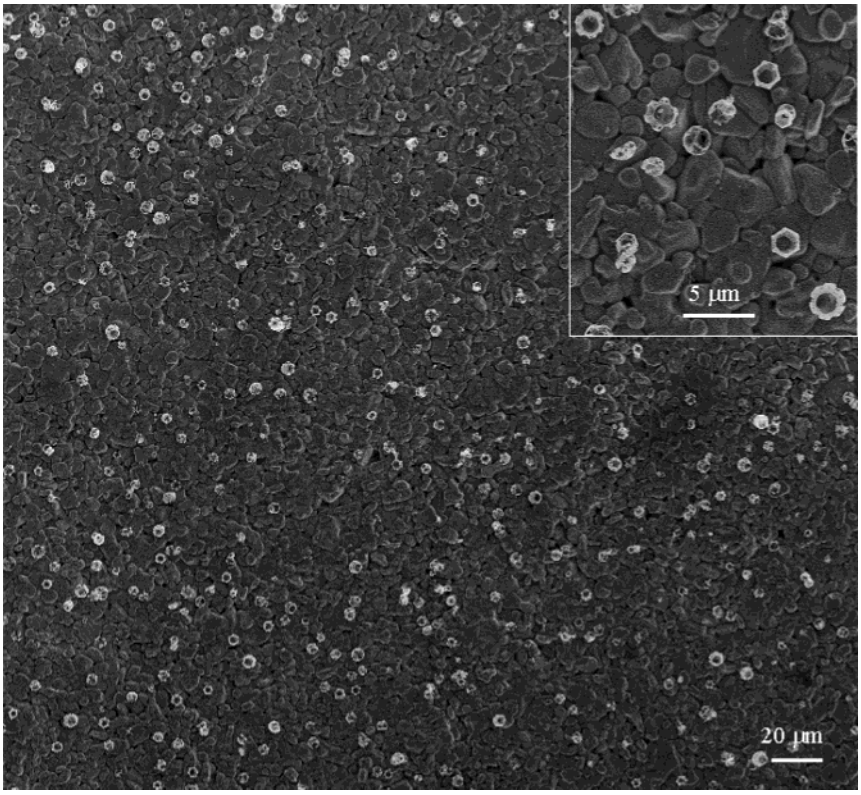

Figure 1. A typical low-magnification SEM image of the as-synthesized ZnO polyhedral cages and shells distributed uniformly on the substrate surface, showing high controllability of the process.

cubic centimeters per minute), and then the tube was cooled to 1000 °C and kept isothermal for 30 min without supplying Ar gas. The gray-white products collected downstream in a temperature range of 300−500 °C onto an alumina substrate are investigated by electron microscopy.

3. Results and Discussions

3.1. Textured Cage and Shell Structures. For a typical synthesis, particles are observed to be dispersed uniformly on an alumina substrate (Figure 1). This process has very high repeatability following the procedures given in the Experimental Section. The dispersive distribution of the particles suggests that they were formed by individual nucleation and growth. A closer examination of the particles indicated that they are mostly hollow shells as presented in the enlarged image inserted in Figure 1, where some polyhedral cages and spherical shells are observed.

In the temperature zone that we are interested in, balls and polyhedra are observed, some of them are dispersed on the substrate, and there appears to be no correlation among them (Figure 2A), while some of them line up along a ZnO nanobelt (Figure 2B) that was formed in a higher temperature zone of typically 700−900 °C. Details about the nanobelts have been reported previously.[21] The nanostructures displayed by the scanning electron microscopy (SEM) images apparently exhibit the regular polyhedral shapes. The typical shapes observed are classified into two groups: hexagon-based drums and spherical/hemispherical shells.

To investigate the related shapes of the cages and shell, we have collected all of the possibly observed shapes through SEM observation to find their common characteristics for proposing a growth mechanism, and the results are collected in Figure 2C−K. The hexagon-based rods are often seen (Figure 2C), but they have the shell structure; some hexagon-based rods with truncated edges are also found (Figure 2D), which have a shape analogous to a drum. The polyhedron is enclosed by (0001) (top and bottom surface), $\{10\bar{1}0\}$ (side surfaces), stepped $\{10\bar{1}1\}$ (inclined surfaces), and high index planes with rough surfaces (Figure 2D and E). Some truncated hexagon-based drums show open corners, as the one displayed in Figure 2F. In some cases, one side of the shell collapses possibly due to high growth temperature as well as the small shell thickness (Figure 2G). The local thickness of the shell depends on the crystallographic nature of the surface; the {0001} surface can be open (Figure 2H−K), and the lower energy $\{10\bar{1}0\}$ surfaces can also be open in some cases (Figure 2I, K). A common feature is that the shell exhibits mesoporous structure, which will be discussed next.

Although the polyhedral shell structure appears to be composed of nanocrystals, transmission electron diffraction and imaging indicates that they have a "single crystalline" textured orientation (Figure 3A), and the side surfaces are $\{10\bar{1}0\}$. The three-dimensionally projected structure can be seen through a bright-field TEM image. A dark-field TEM image confirms that the shell structure is composed of nanocrystals, which are oriented with texturing (Figure 3B). The high-resolution TEM image recorded along [0001] clearly shows the six-fold symmetric lattice image. A detailed analysis of the image indicates grain boundaries, as indicated by arrowheads, and holes introduced by the mesoporous structure (Figure 3C). The average size of the nanocrystals is 20−40 nm.

To trace the effect of Sn in the growth of the cages and shells, a detailed TEM analysis was carried out. There are numerous

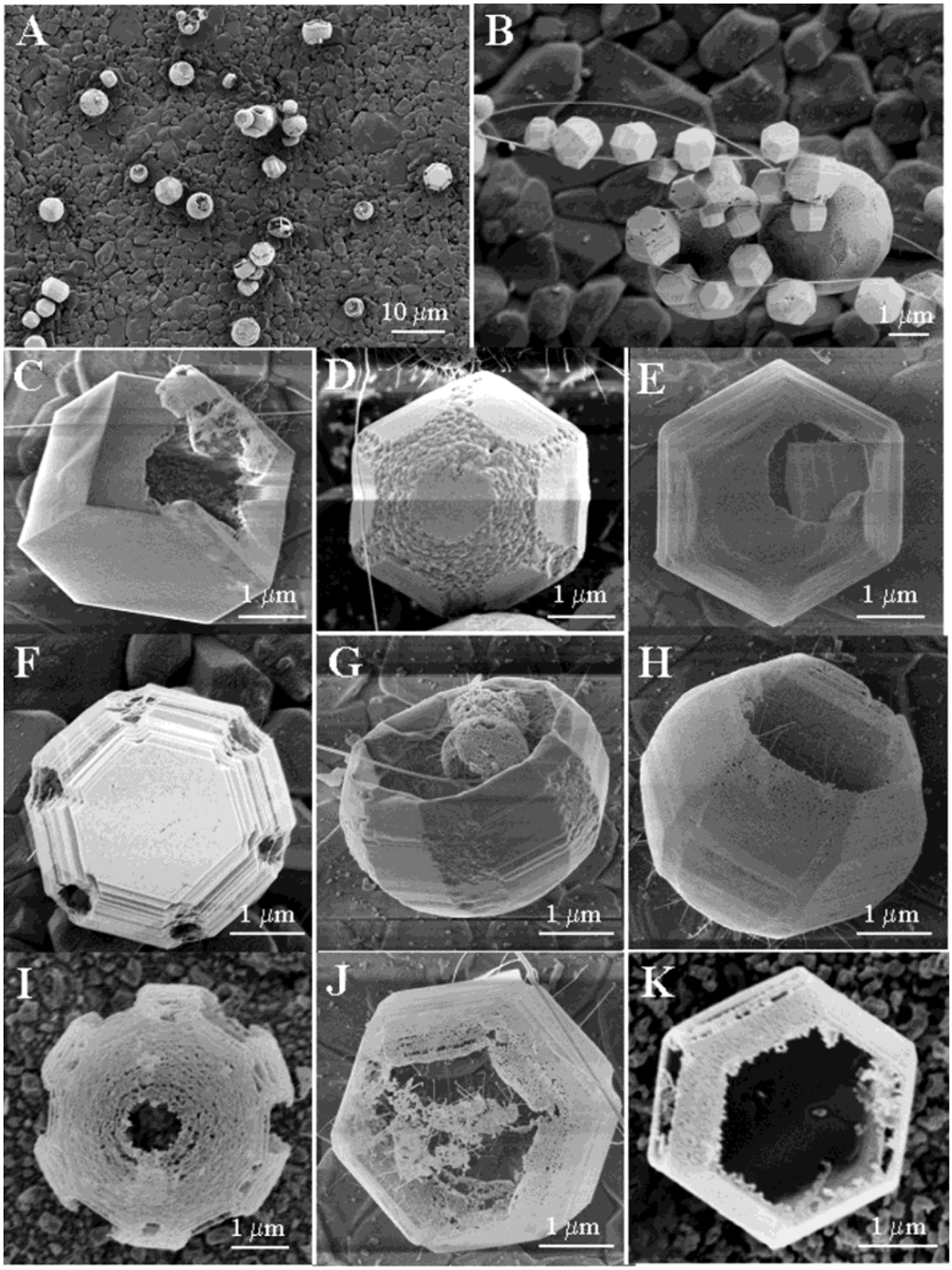

Figure 2. Low-magnification SEM images of ZnO polyhedral cages and shells distributed (A) dispersively on the substrate and (B) aligned along a nanobelt, respectively. (C−E) Typical drum-shaped cages of truncated hexagon-based shells. (F−K) Open cage structures of mesoporous textured ZnO nanocrystals.

ZnO nanowires growing on the surfaces of the cages and shells (Figure 3D). There are usually tiny Sn particles located at the growth front, which lead to the growth of the ZnO nanowires (Figure 3E).[28] EDS analysis, with a detection limit of 2 at. %, shows that the ZnO nanostructure has no Sn content in its volume.

Another major structure observed is the spherical or hemispherical shell structure (Figure 4A), which tends to align along a ZnO nanobelt. Enlargement of the shell clearly presents the mesoporous structure with some open holes (Figure 4B). Spheres with thicker walls can also be identified (Figure 4C); an enlarged SEM image from the surface displays the mesoporous structure

(22) Dai, Z. R.; Pan, Z. W.; Wang, Z. L. *J. Am. Chem. Soc.* **2002**, *124*, 8673−8680.
(23) Hu, J. Q.; Li, Q.; Meng, X. M.; Lee, C. S.; Lee, S. T. *Chem. Mater.* **2003**, *15*, 305−308.
(24) Wu, J. J.; Liu, S. C.; Wu, C. T.; Chen, K. H.; Chen, L. C. *Appl. Phys. Lett.* **2002**, *81*, 1312−1314.
(25) Gallaso, F. *Structure and Properties of Inorganic Solids*; Pergamon Press: New York, 1970.
(26) Uyeda, R. The morphology of fine metal crystals. *J. Cryst. Growth* **1974**, *24/25*, 69.
(27) Petford-Long, A. K.; Smith, D. J. *J. Cryst. Growth* **1987**, *80*, 218−224.
(28) Gao, P. X.; Wang, Z. L. *J. Phys. Chem. B* **2002**, *106*, 12653−12658.

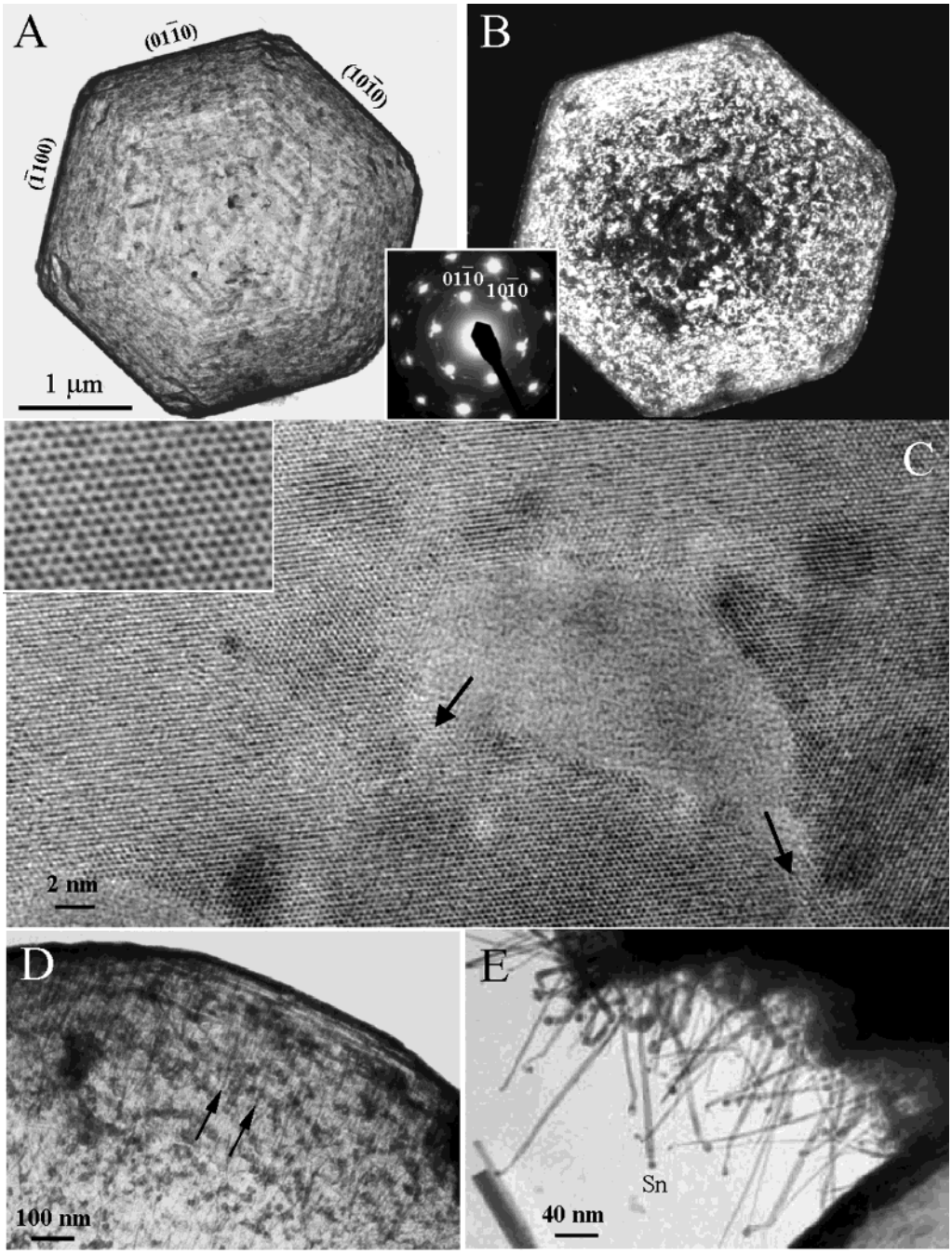

Figure 3. (A) Bright-field and (B) dark-field TEM images of a hexagon-based cage, where the inset electron diffraction pattern shows the textured orientation of the ZnO nanocrystals. (C) High-resolution TEM image recorded along [0001], showing the crystalline, mesoporous, and textured grain structures of the cage. An enlargement of the image is inserted. (D) Low-magnification TEM image showing the growth of ZnO nanowires inside the cage structure, as indicated by arrowheads. (E) TEM image of the ZnO nanowires grown outside of the cage with Sn particles at the tips.

(Figure 4E), with nanocrystallites of sizes ~30 nm. The materials that fill in the sphere are also mesoporous with the presence of ZnO nanowires growing both inside and outside of the shell (Figure 4D). A bright-field TEM image proves the shell structure of the sphere, and the shell thickness is ~50 nm (Figure 4F). The patchy and grainy type contrast observed in the dark-field TEM image (Figure 4G) proves that the shell is nanostructured. The electron diffraction pattern from the shell shows a single crystalline structure and is indexed to be [$\bar{2}$4$\bar{2}$3], confirming the texture of the ZnO nanocrystals.

3.2. Growth Mechanism. The formation process of the polyhedral ZnO shell and cage structures is proposed to be a process comprised of solidification of liquid droplets, surface oxidation, and sublimation (Figure 5). The introduction of graphite in the raw materials is to reduce the oxides into metals as given by

$$2ZnO\ (s) + C\ (s) \rightarrow 2Zn\ (g) + CO_2\ (g) \quad (1)$$

$$SnO_2\ (s) + C\ (s) \rightarrow SnO\ (g) + CO\ (g) \quad (2)$$

$$SnO_2\ (s) + C\ (s) \rightarrow Sn\ (g) + CO_2\ (g) \quad (3)$$

On the basis of our previous study,[22] the SnO vapor can be converted into Sn and SnO_2 vapor at temperatures as low as

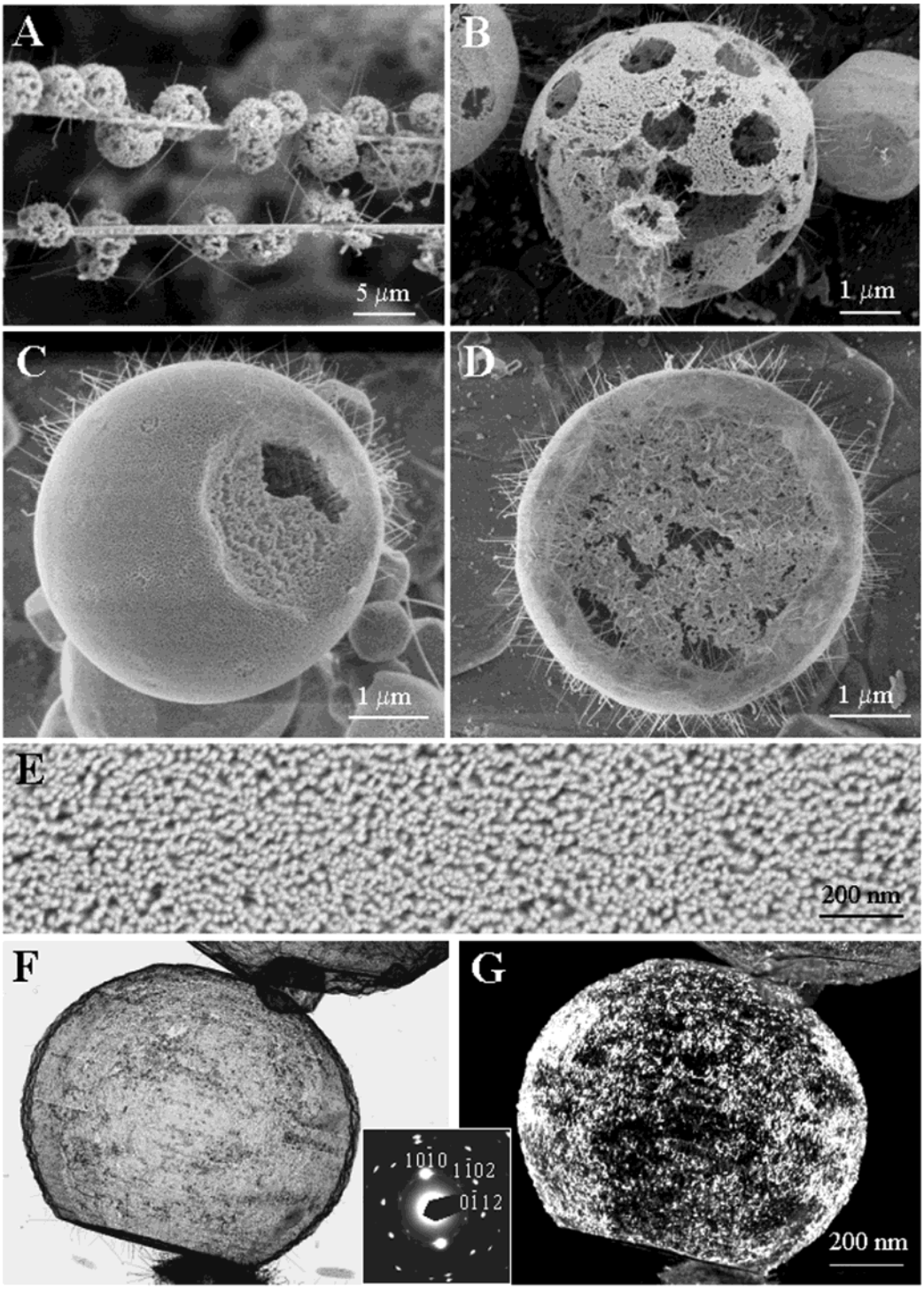

Figure 4. (A) Low-magnification SEM image of spherical shells distributed along a ZnO nanobelt. (B−D) Spherical shells composed of textured ZnO nanocrystals. (E) A high-magnification SEM image from the shell, showing mesoporous and nanostructured nature of the shell. (F, G) Bright-field and dark-field TEM images from a partial hemispherical shell. The corresponding electron diffraction pattern proves the textured orientation of the ZnO nanocrystals in the shell.

900 °C:

$$2SnO\ (g) \rightarrow Sn\ (l) + SnO_2\ (s) \qquad (4)$$

The sublimated Zn atoms are carried downstream by the Ar carrier gas. If the Ar flow gas is turned off during the growth, the concentration of the Zn vapor increases, and in the lower temperature region, Zn atoms condense and form liquid clusters (Figure 5A), which tend to deposit fairly uniformly onto either the substrate or the surface of the nanobelts, formed in the high temperature zone and carried to the lower temperature zone by the Ar gas. The liquid droplets quickly solidify on the substrate in the lower temperature zone, forming faceted single crystalline Zn polyhedra, which are enclosed by {0001}, {10$\bar{1}$0}, and {10$\bar{1}$1} facets (Figure 5B). The residual oxygen in the growth chamber can then oxidize the surface of the Zn polyhedron.[23,24]

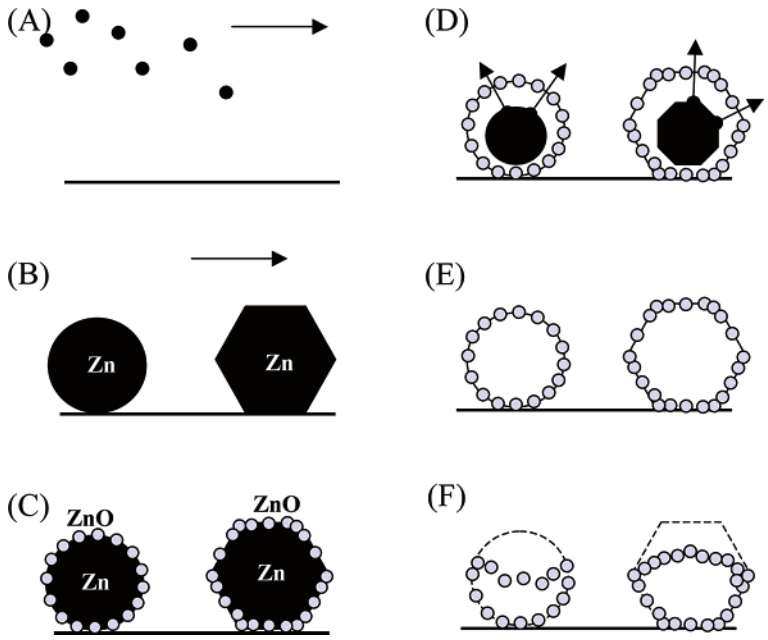

Figure 5. A proposed growth mechanism for the formation of the cages and shells composed of textured ZnO nanocrystals. (A) Zn vapor phase carried by the Ar gas. (B) Deposition of the Zn droplets at a different substrate temperature region results in the formation of single crystalline spherical and hexagon-based rod Zn particles. (C) Surface oxidation produces textured ZnO nanocrystals on the Zn surface. (D, E) Vaporization/sublimation of the Zn core results in the formation of a ZnO cage/shell structure. (F) The cage/shell could collapse due to sintering at the growth temperature.

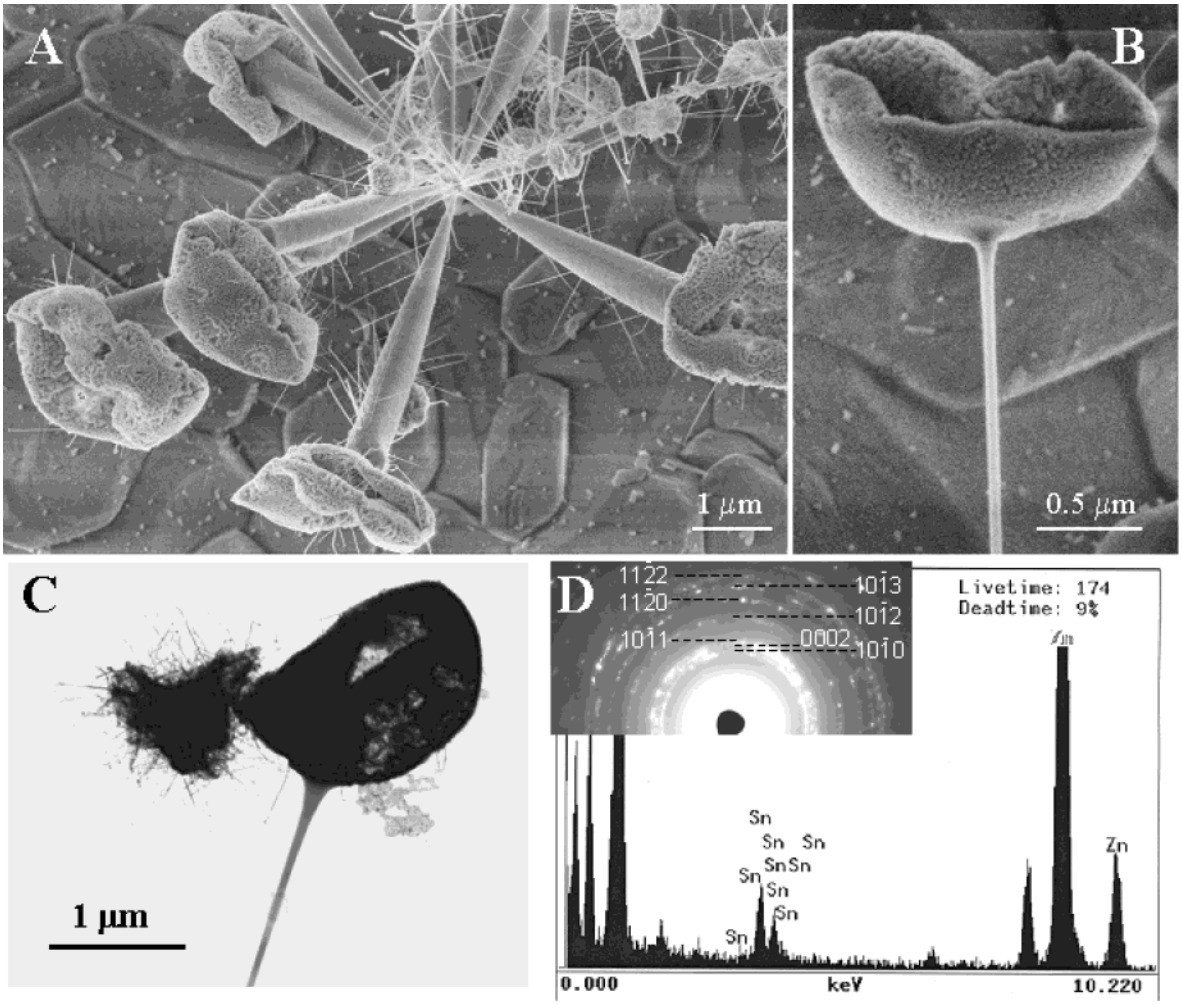

Figure 6. (A) ZnO rods supported Zn−Sn−O "flower"-like structures. (B) A high-magnification TEM image of the structure. (C) TEM image of the structure, and (D) corresponding electron diffraction pattern and EDS spectrum from the top flower region, showing a polycrystalline structure without texturing. The electron diffraction pattern matches very well to the X-ray diffraction data for wurtzite structured ZnO, suggesting the Sn may be present in the form of tiny clusters.

Because the oxidation rates on different crystal surfaces are different, the surface with the lowest energy tends to be most stable and may resist being oxidized, while the high energy surfaces will be quickly oxidized, resulting in the formation of an oxide layer with a nonuniform thickness on the Zn polyhedral surface (Figure 5C). Both Zn and ZnO have the hexagonal crystal structure with lattice constants of $a = 0.2665$, $c = 0.4947$ and $a = 0.3249$, $c = 0.5206$ nm,[25] respectively. ZnO tends to have an epitaxial orientation relationship with the base crystal Zn. Yet the large lattice mismatch of 23.7% in the basal plane makes it impossible to form large size ZnO crystals covering the Zn surface. Instead, ZnO nanocrystallites are formed as islands, and they preserve the same orientation as the Zn crystal and leave gaps/pores between the nanocrystallites because of large local mismatch strain. The mesoporous structure is formed due to the distribution and growth of multinuclei on the Zn surface. Moreover, Zn has a much lower melting point of 419 °C than that of 1975 °C for ZnO; an increase in local temperature between 300 and 500 °C during the growth leads to the sublimation of Zn but not ZnO (Figure 5D),[23] resulting in the formation of the textured ZnO shell/cage structure (Figure 5E). In some cases, the shell collapsed after the vaporization of the Zn core possibly because the oxide layer is thin and the local temperature is high enough to cause sintering (Figure 5F), forming various collapsed structures observed by SEM.

The temperature gradient may determine the equilibrium shapes for original Zn particles and the subsequent shapes of the nanostructured ZnO shells/cages (Figure 5B−F). At a lower temperature region (below the melting point of Zn, 419 °C), the cages tend to have equilibrium shapes enclosed by (0001), $\{10\bar{1}0\}$, and $\{10\bar{1}1\}$ faces with relatively lower energy[26] due to a more spontaneous solidification process. In a higher temperature region (close to or above the melting point of Zn, 419 °C), spherical-like shells/cages may be formed due to the small undercooling level for the solidification process, with an appreciable tendency to remain as spherical-shaped liquid droplets[26,27] while their surfaces are being oxidized.

3.3. "Flower"-like Structure and Tin Content. The reduced Sn metal would serve as a catalyst for the growth of ZnO nanowires[28] inside and outside of the ZnO shell/cage (Figure 4). Energy-dispersive X-ray spectroscopy (EDS) chemical analysis from the polyhedral shell structure indicates that the content of Sn is, if any, less than the EDS detection limit of typically 1−2 at. %. To trace the distribution of Sn in the final products, all of the structural configurations have been examined by EDS. Figure 5A shows the growth of a "flower"-like structure, where the branches are ZnO rods growing along [0001] (Figure 6B), and the "flower" is a nanocrystal composite (Figure 6C) with Sn content of ∼8 at. %. Electron diffraction from the "flower" shows that the nanocrystals are oriented randomly, distinctly different from the cage and shell structures presented in Figures 1−4, but the diffraction pattern still fits the ZnO structure. It may be suggested that the Sn could be present in tiny particles mixed in the nanocrystals that compose the "flower"-like structure. It must be pointed out that the "flower"-like structure was observed only occasionally. The structure observed in Figure 6A is the sintering result of the collapsed Zn−Sn−O shells after the vaporization of the Zn core.

4. Conclusions

We have reported a new structure, mesoporous structured polyhedral drum and spherical cages and shells formed by textured self-assembly of ZnO nanocrystals, which are made by a novel self-assembly process during epitaxial surface oxidation. The cages/shells exhibit unique geometrical shapes, and their walls are composed of mesoporous and textured ZnO nanocrystals. The structures of the cages and shells are studied, and a growth mechanism is proposed to be a process following solidification of the Zn liquid droplets, surface oxidation, and sublimation.

Acknowledgment. The authors acknowledge support from the NASA URETI program.

JA035569P